ACTA ACUSTICA UNITED WITH ACUSTICA
Vol. 88 (2002) 463 – 471

Three-dimensional non-reflective boundary conditions for acoustic simulations: far field formulation and validation test cases

C. Bogey, C. Bailly
Laboratoire de Mécanique des Fluides et d'Acoustique, UMR CNRS 5509 & Ecole Centrale de Lyon, BP 163, 69131 Ecully, France

Summary
In aeroacoustic simulations, non-reflective boundary conditions are necessary to minimize the acoustic waves reflected when disturbances leave the computational domain. In the present paper, far field boundary conditions are developed for a 3-D geometry. Two validation test cases involving respectively an acoustic pulse and an axisymmetric ring vortex in a uniform mean flow are also proposed. The solutions from linearized Euler equations show that the far field boundary conditions allow the exit of acoustic waves without generating significant spurious waves. The exit of vortical disturbances is more difficult to treat with efficiency because of their high magnitude. For this case, the implementation of a sponge zone is presented to decrease the amplitude of acoustic reflections.

PACS no. 43.20.Bi, 43.28.Ra

1. Introduction

In numerical simulations of exterior problems, a set of equations is required to model the free field conditions. These boundary conditions are applied as in Figure 1, all around the interior computational domain where the flow motion equations, namely Navier-Stokes or Euler equations, are solved. They must allow the flow disturbances to leave the computational domain without significant reflections. This point is crucial in computational aeroacoustics [1], since spurious acoustic waves generated by poor boundary conditions may mask the physical sound field radiated by turbulence. Advanced non-reflective boundary conditions have thus been developed [2], so that the computation of the sound field directly from Navier-Stokes simulations [3, 4, 5, 6] is now possible. These conditions can be classified into two main approaches.

The first one is based on characteristics. It has been clearly developed by Thompson [7, 8], and Poinsot and Lele [9], and is widely used in computational fluid dynamics. The basic idea is to recast the hyperbolic system associated to the Eulerian fluxes in the direction perpendicular to the boundary, in terms of the Riemann invariants related to vortical, entropic and acoustic perturbations. The treatment of the boundary can then be performed by calculating the outgoing invariants using non-centered numerical scheme and by imposing the value of incoming invariants. Typically, to simulate a free field boundary condition, the value of incoming invariants is set to zero. This method is intrinsically 1-D, and is efficient for perturbations reaching the boundaries perpendicularly. It is however badly suited to oblique incidences, and there is a discontinuity in the treatment of boundaries in the corners of the computational domain. An improvement of the characteristic method accounting for the effects of oblique incidences has been proposed by Giles [10], and it has been discussed by Colonius *et al.* [11].

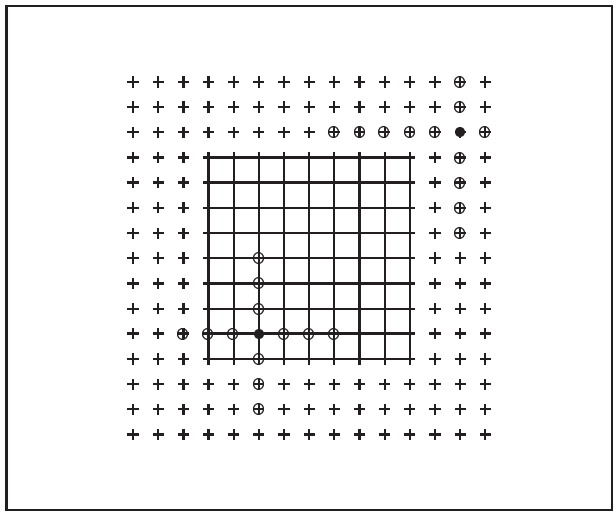

Figure 1. Computational domain: ——— interior domain (Navier-Stokes or Euler equations); – – – boundary domain. To evaluate derivatives at points • with a seven point stencil scheme, points ○ are used.

Received 13 July 2001,
accepted 22 March 2002.

The second approach suggested by Bayliss and Turkel [12] consists in building boundary conditions for far field radiation. In this way, Tam and Webb [13] have developed two-dimensional non reflective boundary conditions by using far field asymptotic expressions of Euler's equations linearized around a uniform mean flow. These conditions have been later extended for a non uniform mean flow by Tam and Dong [14]. This formulation, written in polar coordinates for a 2-D geometry, is multidimensional. This ensures a continuous treatment along all the boundaries, which is one of the main differences with characteristics. The Thompson, Giles, and Tam and Webb boundary conditions have been tested by Hixon *et al.* [15] in the case of an acoustic monopolar source in a uniform mean flow, and reflected sound waves have been found to be smaller with Tam and Webb conditions.

This paper has two objectives relative to non-reflective boundary conditions for aeroacoustic simulations. The first one is to develop a far field formulation of these conditions for a 3-D geometry, by extending the work of Tam and Dong. The second objective is to propose validation test cases to evaluate the efficiency of 3-D free field conditions in minimizing acoustic reflections. The exit from the computational domain of two kinds of disturbances, acoustic and vortical, is considered with two problems involving respectively an acoustic pulse and an axisymmetric ring vortex in a uniform flow. These two problems are solved in the present paper using a Linearized Euler Equations (LEE) solver. The far field conditions provide good numerical results, but a damping zone is still required to treat the exit of vortical fluctuations in acoustic simulations.

The far field formulation of boundary conditions is developed in section 2, with two sets of equations corresponding to radiation or outflow conditions. In section 3, the two test cases are defined: a Gaussian acoustic pulse and an axisymmetric vortex, placed in a uniform flow with Mach number $\mathrm{M} = 0.5$. Both are solved to evaluate the accuracy of the far field boundary conditions. In section 4, a damping zone is implemented at the outflow boundary to minimize the reflected waves for the second test case. Concluding remarks are given in section 5. The analytical solution of the acoustic pulse is provided in the appendix.

2. Far field formulation of three- dimensional boundary conditions

The far field boundary conditions derived by Tam and Dong [14] in two dimensions are generalized to three dimensions. Acoustic and aerodynamic disturbances generated by turbulent flows behave quite differently: sound waves propagate in all the directions at a velocity equal to the sum of the sound speed and of the flow velocity, whereas entropic and vortical perturbations are only convected downstream by the flow. Two free field formulations are therefore required: radiation conditions for boundaries reached by acoustic waves alone, and outflow conditions for boundaries where all kinds of disturbances

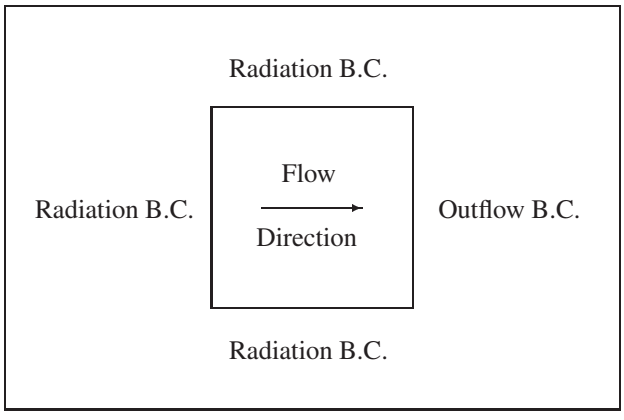

Figure 2. Sketch of the boundary conditions. Radiation conditions are applied in the right corner regions.

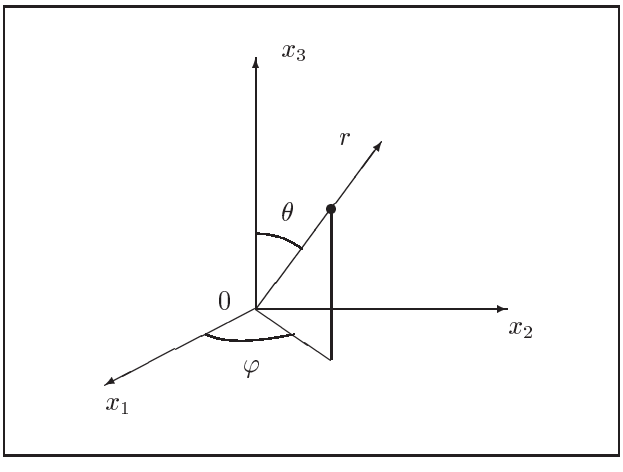

Figure 3. Spherical coordinates used to formulate 3-D boundary conditions.

can be found. A sketch of the boundary configuration is shown in Figure 2.

In order to make boundary conditions suitable to the spherical three-dimensional acoustic waves, spherical coordinates (r, θ, φ) are used, as illustrated in Figure 3. These coordinates are defined from an origin $\mathrm{O}(x_o, y_o, z_o)$ assumed to be close to the location of the acoustic sources, with three unit vectors $(\mathbf{e}_r, \mathbf{e}_\theta, \mathbf{e}_\varphi)$ in the r, θ and φ directions given in cartesian coordinates by:

$$\begin{cases} \mathbf{e}_r = (\sin\theta\cos\varphi, \sin\theta\sin\varphi, \cos\theta) \\ \mathbf{e}_\theta = (\cos\theta\cos\varphi, \cos\theta\sin\varphi, -\sin\theta) \\ \mathbf{e}_\varphi = (-\sin\varphi, \cos\varphi, 0) \end{cases} \tag{1}$$

The speed of wave propagation, $v_g\mathbf{e}_r$, is the vector sum of the mean sound speed $\bar{\mathbf{c}}$ and of the mean flow velocity $\overline{\mathbf{u}} = (\overline{u}_1, \overline{u}_2, \overline{u}_3)$, as shown by the velocity vector diagram of Figure 4. To find its full expression, the vectors are projected in the sound propagation direction $\mathbf{e}_r$:

$$\begin{aligned} v_g &= (\overline{\mathbf{u}} + \overline{\mathbf{c}}) \cdot \mathbf{e}_r \\ &= \overline{\mathbf{u}} \cdot \mathbf{e}_r + \sqrt{\overline{c}^2 - (\overline{\mathbf{u}} \cdot \mathbf{e}_\theta)^2 - (\overline{\mathbf{u}} \cdot \mathbf{e}_\varphi)^2} \end{aligned} \tag{2}$$

To formulate the boundary conditions, the fluctuating field is decomposed into entropic, vortical and acoustic

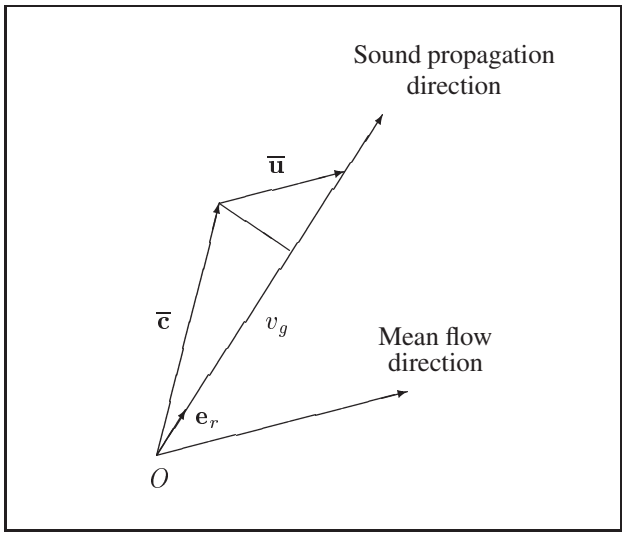

Figure 4. Speed of wave propagation v_g.

modes. The three modes are assumed to be independent, which is exact only for a uniform mean flow or in a geometrical approximation for high-frequency perturbations. For a mean flow $(\overline{\rho}, \overline{\mathbf{u}}, \overline{p})$, the fluctuating field $(\rho', \mathbf{u}', p')$ can then be written as the sum of acoustic, vortical and entropic waves:

$$\begin{pmatrix} \rho' \\ \mathbf{u}' \\ p' \end{pmatrix} = \begin{pmatrix} \rho_a \\ \mathbf{u}_a \\ p_a \end{pmatrix} + \begin{pmatrix} 0 \\ \psi \\ 0 \end{pmatrix} + \begin{pmatrix} \chi \\ 0 \\ 0 \end{pmatrix} \tag{3}$$

where $\psi = \psi(\mathbf{x} - \bar{\mathbf{u}}t)$ and $\chi = \chi(\mathbf{x} - \bar{\mathbf{u}}t)$. To model the boundary conditions, the far-field expression of the acoustic disturbances $(\rho_a, \mathbf{u}_a, p_a)$ is used. For a 3-D geometry, we have:

$$\begin{pmatrix} \rho_a \\ \mathbf{u}_a \\ p_a \end{pmatrix} \sim \frac{F\left(r/v_g - t\right)}{r} \begin{pmatrix} 1/\overline{c}^2 \\ \left(1/\overline{\rho}\,\overline{c}\right)\mathbf{e}_r \\ 1 \end{pmatrix}. \tag{4}$$

2.1. Radiation boundary conditions

When only acoustic disturbances reach the boundary, the perturbations are given by (3) with $\psi = 0$ and $\chi = 0$. The radiation conditions are then found by deriving the differential equation satisfied by the acoustic disturbances (4). This leads to:

$$\frac{\partial}{\partial t}\begin{pmatrix} \rho' \\ \mathbf{u}' \\ p' \end{pmatrix} + v_g \left(\frac{\partial}{\partial r} + \frac{1}{r}\right)\begin{pmatrix} \rho' \\ \mathbf{u}' \\ p' \end{pmatrix} = 0. \tag{5}$$

This equation is integrated for the points located in the boundary domain by using the same time integration as for the interior points, but with non-centered schemes for spatial derivation as shown in Figure 1. The same equation is solved for all the radiation boundaries and in this way, there is no discontinuity between two connected neighbouring boundaries, and no specific implementation for corners is needed.

2.2. Outflow boundary conditions

At the outflow, the full expression (3) must be considered since both aerodynamic and acoustic disturbances reach the boundary. The pressure fluctuations are associated with acoustic waves alone, i.e. $p' = p_a$, and the previous differential equation (5) is kept for the fluctuating pressure:

$$\frac{\partial p'}{\partial t} + v_g \left(\frac{\partial}{\partial r} + \frac{1}{r}\right) p' = 0$$

From equation (3), the density and velocity perturbations satisfy:

$$\begin{cases} \dfrac{\partial \rho'}{\partial t} + \overline{\mathbf{u}}.\nabla\rho' = \dfrac{\partial \rho_a}{\partial t} + \overline{\mathbf{u}}.\nabla\rho_a \\ \dfrac{\partial \mathbf{u}'}{\partial t} + \overline{\mathbf{u}}.\nabla\mathbf{u}' = \dfrac{\partial \mathbf{u}_a}{\partial t} + \overline{\mathbf{u}}.\nabla\mathbf{u}_a \end{cases}$$

By using the assumption of isentropic acoustic perturbations, i.e. $\rho_a = p_a/\overline{c}^2$, we get for the density equation:

$$\frac{\partial \rho'}{\partial t} + \overline{\mathbf{u}}.\nabla\rho' = \frac{1}{\overline{c}^2}\left(\frac{\partial p_a}{\partial t} + \overline{\mathbf{u}}.\nabla p_a\right).$$

Since the acoustic perturbations satisfy the momentum equations of the linearized Euler equations, the velocity equation become:

$$\frac{\partial \mathbf{u}'}{\partial t} + \overline{\mathbf{u}}.\nabla\mathbf{u}' = -\frac{1}{\overline{\rho}}\nabla p_a.$$

By reminding that $p' = p_a$, the set of equations solved in the outflow region is then given by:

$$\begin{cases} \dfrac{\partial \rho'}{\partial t} + \overline{\mathbf{u}}.\nabla\rho' = \dfrac{1}{\overline{c}^2}\left(\dfrac{\partial p'}{\partial t} + \overline{\mathbf{u}}.\nabla p'\right) \\ \dfrac{\partial \mathbf{u}'}{\partial t} + \overline{\mathbf{u}}.\nabla\mathbf{u}' = -\dfrac{1}{\overline{\rho}}\nabla p' \\ \dfrac{\partial p'}{\partial t} + v_g\left(\dfrac{\partial}{\partial r} + \dfrac{1}{r}\right)p' = 0. \end{cases} \tag{6}$$

3. Validation test cases

To determine which of the numerical methods can be used to calculate sound waves with a high accuracy, test cases specific to Computational AeroAcoustics (CAA) [16, 17, 18] have been developed recently. In the same way as the first ICASE/LaRC Workshop has provided two-dimensional test cases [16] to evaluate the efficiency of non-reflective boundary conditions, the present paper proposes two test cases for three-dimensional problems. To test the free-field boundary conditions, the exit of acoustic and vortical disturbances from the computational domain is considered, with first a Gaussian acoustic pulse and second an axisymmetric ring vortex, both being placed in a uniform flow.

The two test cases can be solved from Navier-Stokes or Euler equations. For example, they have been used to develop a Large Eddy Simulation code [19] to compute directly the sound field radiated by turbulent flows [5, 6].

In the present paper, their solutions from Linearized Euler's equations are reported. The LEE solver (SPRINT for Sound Propagation IN Turbulence) is built up to study sound propagation, with the far field boundary conditions described in section 2. In this solver, the Dispersion-Relation-Preserving (DRP) finite difference scheme proposed by Tam and Webb [13] is used for spatial discretization because of its very small dispersion, and time integration is carried out by a fourth-order Runge-Kutta algorithm. A selective damping is also applied at every iteration to filter out numerical grid-to-grid oscillations. More details and validations of the two-dimensional version of the code can be found in [20]. The far field boundary conditions are applied as shown in Figure 1, by using DRP non-centered schemes [21] in three points. They are advanced in time by the same Runge-Kutta algorithm as for the Linearized Euler equations themselves.

Density, velocity and pressure in LEE are decomposed in mean values $\overline{\rho}$, $\overline{\mathbf{u}} = (\overline{u}_1, \overline{u}_2, \overline{u}_3)$ and $\overline{p}$, and in fluctuating values ρ', $\mathbf{u}' = (u'_1, u'_2, u'_3)$ and p'. In what follows, all the variables are nondimensionalized by the scales:

length scale	: Δ	
velocity scale	: c_∞	(ambient sound speed)
time scale	: Δ/c_∞	
density scale	: ρ_∞	(ambient density)
pressure scale	: $\rho_\infty c_\infty^2$	

where Δ is the constant mesh size. The computational domain defined by a N^3 uniform grid with $N = 101$ is such that $-50 \leq x_1, x_2, x_3 \leq 50$. The origin of the spherical coordinates used for the boundary conditions is at $O(0,0,0)$ and corresponds to the initial source location in the two problems. To estimate the magnitude of acoustic waves reflected back into the computational domain after the exit of disturbances, the time evolution of the residual fluctuating pressure L_p is recorded. This residual pressure is based on the following L_2 norm:

$$L_p = \left[\frac{1}{N^3} \sum_{i,j,k}^{N^3} p'^2_{i,j,k} \right]^{1/2}.$$

All the computations are performed in double precision.

3.1. Gaussian acoustic pulse in a uniform flow

We first study the propagation of an initial Gaussian acoustic pulse placed in a uniform flow $\overline{\mathbf{u}} = (\mathrm{M}, 0, 0)$ with constant mean density $\overline{\rho} = 1$ and pressure $\overline{p} = 1/\gamma$, as shown in Figure 5. The initial conditions at $t = 0$ are:

$$\begin{aligned} p' &= \epsilon \exp\left[-\alpha\left(x_1^2 + x_2^2 + x_3^2\right)\right], \\ \rho' &= \epsilon \exp\left[-\alpha\left(x_1^2 + x_2^2 + x_3^2\right)\right], \\ u'_1 &= 0, \\ u'_2 &= 0, \\ u'_3 &= 0, \end{aligned}$$

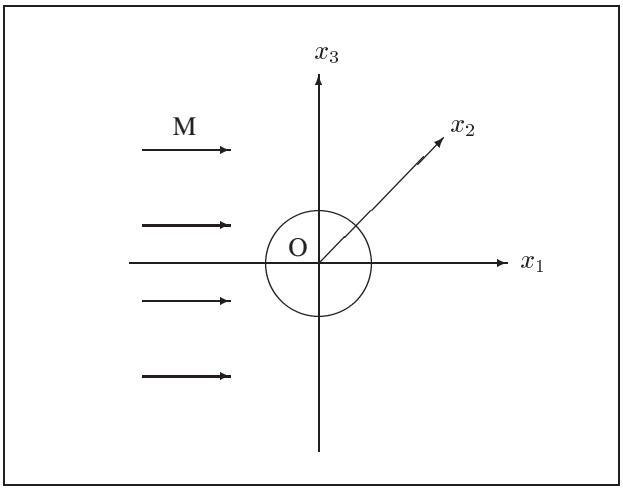

Figure 5. 3-D acoustic pulse in a uniform flow.

where $\alpha = (\ln 2)/b^2$. The flow Mach number is $\mathrm{M} = 0.5$, the Gaussian half-width $b = 3$ and the amplitude $\epsilon = 10^{-3}$.

The analytical solution of this initial value problem is developed in the appendix. It is given by:

$$p'(\mathbf{x}, t) = \frac{\epsilon}{\beta} \int_0^\infty \xi^2 \exp\left[-\frac{\xi^2}{4\alpha}\right] \cos(t\xi)\, \mathrm{j}_0(\xi\eta)\, \mathrm{d}\xi,$$

where:

$$\eta = \left((x_1 - \mathrm{M}t)^2 + x_2^2 + x_3^2\right)^{1/2},$$

and $\beta = 2\alpha\sqrt{\pi\alpha}$. The spherical Bessel function of the first kind and order zero j_0 is given by $\mathrm{j}_0(z) = \sin(z)/z$.

The pressure fields $|p'|/\epsilon$ obtained in the (Ox_1x_2) and (Ox_2x_3) planes are presented in Figures 6 and 7, at times $t = 40$, 80 and 120, and at times $t = 40$ and 80 respectively. The acoustic wave generated by the initial pulse propagates and reaches successively the outflow, lateral and inflow boundaries, at $t = 100/3$, 50 and 100, with amplitudes $|p'|/\epsilon \geq 10^{-2}$. The pressure fields calculated from LEE are compared to the analytical solutions, and contours are in very good agreement. The contour corresponding to the small amplitude of $|p'|/\epsilon = 2.5 \times 10^{-4}$ is hardly modified by possible reflected waves. Thus, the effective reflection rate, defined as the ratio between the amplitude of the acoustic wave when hitting the boundary and the amplitude of the reflected wave is less than 2%.

The time evolution of L_p obtained from LEE is displayed in Figure 8. As long as the acoustic wave generated by the initial pulse is in the computational domain, the value of the residual fluctuating pressure is equal to the analytical solution. Afterwards, for times $t > 150$, the residual pressure L_p is calculated only from parasitic pressure fluctuations such as reflected waves or numerical oscillations, and it is very small, around two orders of magnitude smaller than its initial value. This confirms the great efficiency of the far field formulation of boundary conditions

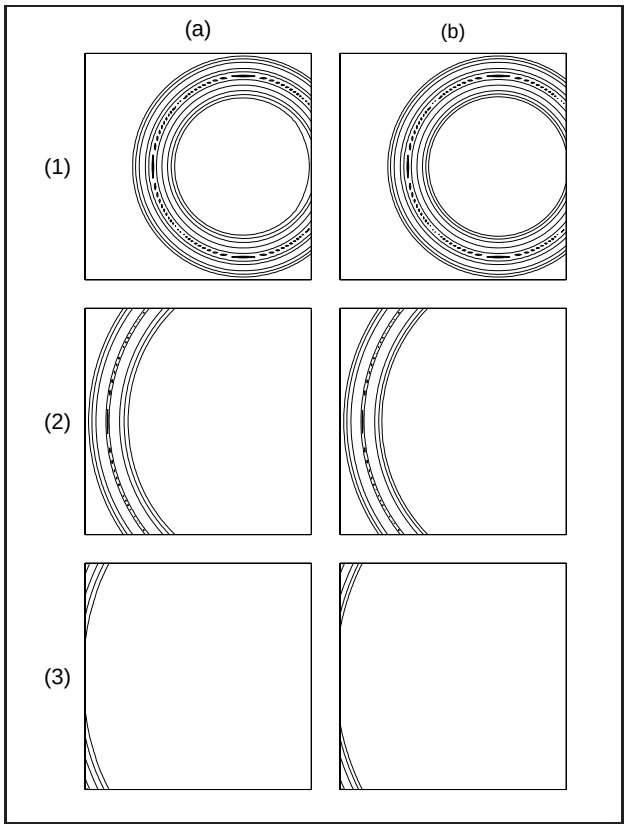

Figure 6. Acoustic pulse in a uniform flow. Pressure fields $|p'|/\epsilon$ obtained in the (Ox_1x_2) plane: (a) from LEE and (b) from the analytical solution, at: (1) $t = 40$, (2) $t = 80$ and (3) $t = 120$. Representation of 4 iso-contours defined by a geometrical ratio of 4 from 2.5×10^{-4} to 1.6×10^{-2}.

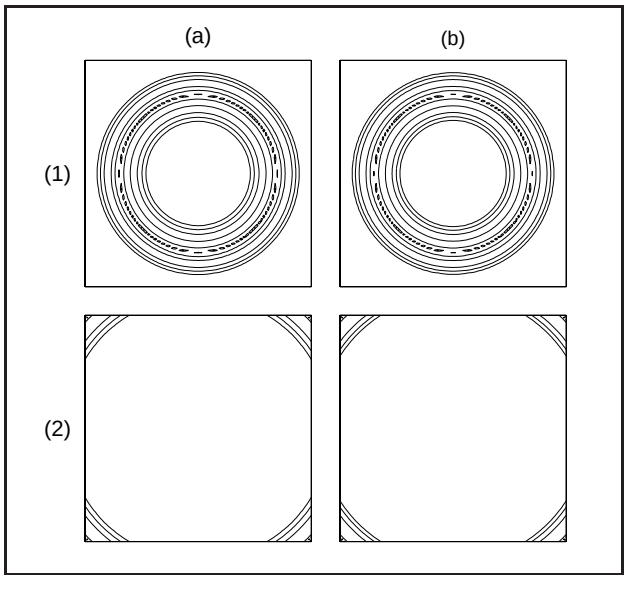

Figure 7. Acoustic pulse in a uniform flow. Pressure fields $|p'|/\epsilon$ obtained in the (Ox_2x_3) plane: (a) from LEE and (b)from the analytical solution, at: (1) $t = 40$ and (2) $t = 80$. Representation of the 4 iso-contours defined in Figure 6.

in allowing the exit of acoustic waves without generating significant reflections.

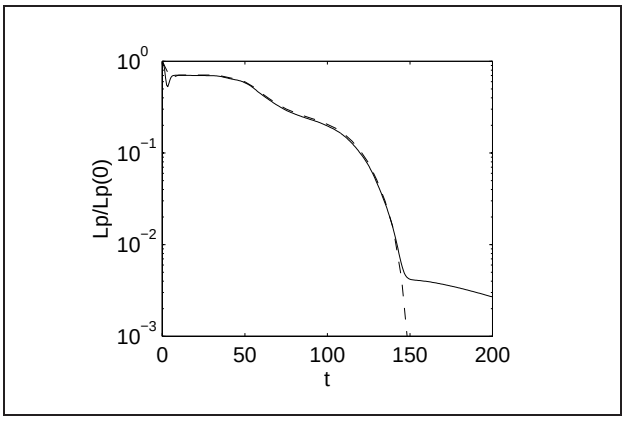

Figure 8. Acoustic pulse in a uniform flow. Time evolution of $L_p/L_p(0)$: ——— LEE solution, – – – analytical solution.

3.2. Axisymmetric vortex in a uniform flow

We now consider the convection of an axisymmetric ring vortex in a uniform flow $\overline{\mathbf{u}} = (\mathrm{M}, 0, 0)$ with constant mean density $\overline{\rho} = 1$ and pressure $\overline{p} = 1/\gamma$, as shown in Figure 9. The axisymmetric vortex is defined at $t = 0$ by the axial and radial velocities u_x^v and u_r^v given by:

$$\begin{cases} u_x^v &= \epsilon \dfrac{r_0}{r}(r - r_0) \exp\left[-\alpha\left(x_1^2 + (r - r_0)^2\right)\right], \\ u_r^v &= -\epsilon \dfrac{r_0}{r} x_1 \exp\left[-\alpha\left(x_1^2 + (r - r_0)^2\right)\right], \end{cases}$$

with:

$$x = x_1 \quad r = \left(x_2^2 + x_3^2\right)^{1/2} \quad \theta = \arctan\left(x_3/x_2\right)$$

and $\alpha = (\ln 2)\,/b^2$. The vortex radius is $r_0 = 20$, the half-width is $b = 5$ and the velocity amplitude is $\epsilon = 0.03$. The flow Mach number is chosen as M=0.5. Thus, the initial conditions of the test case at $t = 0$ are:

$$p' = 0 \quad \rho' = 0 \quad u'_x = u_x^v \quad u'_r = u_r^v \quad u'_\theta = 0$$

The vorticity and pressure fields obtained in the (Ox_1x_2) plane are presented in Figure 10 at times $t = 50$, 100 and 150. The axisymmetric vortex is convected by the uniform mean flow and reaches the outflow boundary at $t = 100$. Afterwards, it leaves completely the computational domain. The corresponding pressure iso-contours show that the exit of the vortex generates acoustic waves with an amplitude around $|p'| \simeq 8 \times 10^{-5}$. Then these waves propagate upstream and contaminate the whole computational domain. They can be compared to the aerodynamic pressure fluctuation p'_{aero} associated with the vortex, and estimated by $u'^2_{max}/2$ where u'_{max} is the maximum velocity in the vortex. In the present simulation, we found $u'_{max} \simeq 8 \times 10^{-2}$ and $p'_{aero} \simeq 3 \times 10^{-3}$. Therefore, the reflection rate is small, around 3%. However, owing to the large difference of magnitude between aerodynamic and acoustic perturbations in turbulent flows, reflections may not be negligible and may mask the physical pressure field.

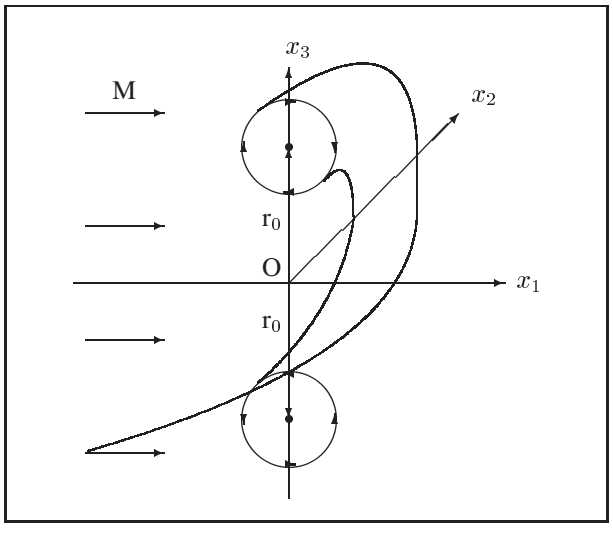

Figure 9. Axisymmetric vortex in a uniform flow. Representation of half the vortex defined by $x_2 > 0$.

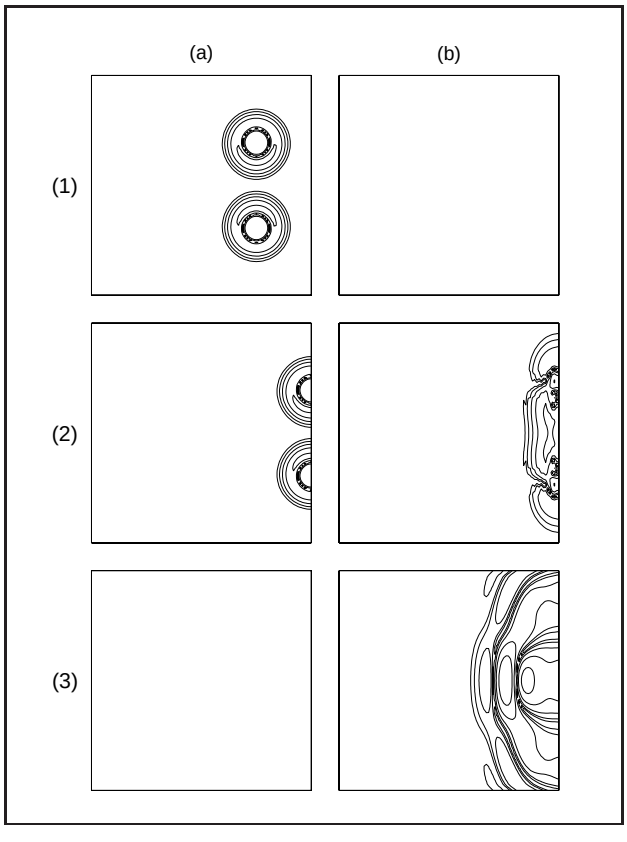

Figure 10. Axisymmetric vortex in a uniform flow. (a) vorticity fields $|\omega_3| = |\partial u_2'/\partial x_1 - \partial u_1'/\partial x_2|$ and (b) pressure fields $|p'|$, obtained in the (Ox_1x_2) plane from LEE at: (1) $t = 50$, (2) $t = 100$ and (3) $t = 150$. Representation of: 5 vorticity iso-contours from 5×10^{-4} to 80×10^{-4}, and 5 pressure iso-contours from 5×10^{-6} to 80×10^{-6}, defined by two geometrical ratios of 2.

The generation of acoustic waves by the outflow boundary is clearly visible in Figure 11 displaying the time evolution of the residual fluctuating pressure L_p. From an initial value of 4×10^{-7} associated to a small acoustic transitional wave, the residual pressure reaches a value of 2×10^{-5} just after the vortex hits the outflow boundary at $t = 100$. Then, it decreases regularly while reflected waves leave progressively the computational domain. The efficiency of the outflow boundary conditions in allowing the exit of vortical perturbations without generating significant spurious acoustic waves is still to be improved. In practice, it is done by adding a sponge zone at the outflow to minimize the amplitude of the reflections.

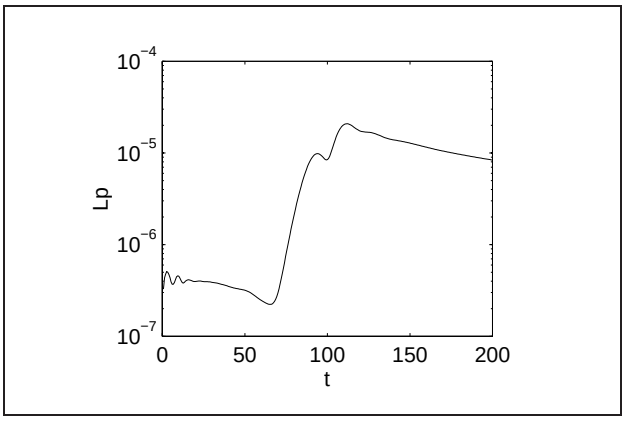

Figure 11. Axisymmetric vortex in a uniform flow. Time evolution of L_p: ——— LEE solution.

4. Application of a damping zone at the outflow boundary

In acoustic simulations involving vortical disturbances, a damping zone is generally used in the vicinity of the outflow boundary to decrease the amplitude of turbulent structures before they reach the boundary, and consequently the amplitude of reflected acoustic waves. With this aim in view, an artificial damping term can be added to the flow motion equations. This is for example the case in the technique called Perfectly Matched Layer developed in [22] and applied for acoustic problems in [23, 24]. The alternative method consists in using a grid stretching so that the turbulent structures no longer supported by the numerical scheme are dissipated. In practice as suggested in [11], it is interesting to combine the two approaches, damping term and grid stretching, to improve the efficiency of the so-called sponge zone.

In this section, the second test case is reexamined using a simple damping zone on the uniform grid defined in section 3.2. The motivation for this is to compare the results with and without damping on the same grid, and thus to study only the effects of the artificial dissipation on the reflected waves. The artificial damping is applied progressively from $x = 15$ to $x = 50$. The width of the sponge zone is arbitrary, but it should be noted that this zone must generally contain a large amount of points, at least 20 points, to be efficient. Every time step $\Delta t = 2/3$, the unknown vector $\mathbf{U}' = [\rho', u_i', p']$ is filtered over the

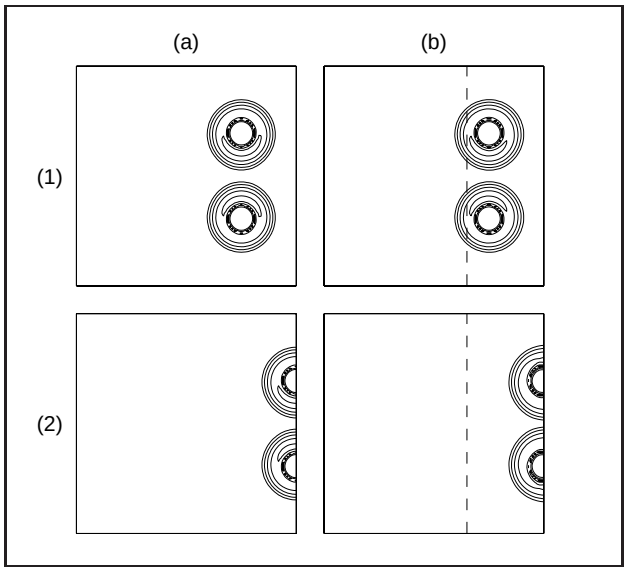

Figure 12. Application of a damping zone. Vorticity fields $|\omega_3|$ obtained in the (Ox_1x_2) plane from LEE: (a) without damping zone and (b) with damping zone at: (1) $t = 50$ and (2) $t = 100$. Representation of the 5 vorticity iso-contours defined in Figure 10. − − − boundary of the damping zone.

last 35 points in the downstream direction to give:

$$\tilde{\mathbf{U}}'_{i,j,k} = \mathbf{U}'_{i,j,k} - \alpha \left(\frac{x_1 - 15}{35}\right)^{\beta} \Big[3d_0 \mathbf{U}'_{i,j,k} + d_1 \Big(\mathbf{U}'_{i+1,j,k} + \mathbf{U}'_{i-1,j,k} + \mathbf{U}'_{i,j+1,k} + \mathbf{U}'_{i,j-1,k} + \mathbf{U}'_{i,j,k+1} + \mathbf{U}'_{i,j,k-1} \Big) \Big],$$

where the magnitude of the filtering is characterized by the amplitude α and the exponent β taken usually such as $0 \leq \alpha \leq 0.3$ and $1 \leq \beta \leq 2$. In the present problem, values of $\alpha = 0.2$ and $\beta = 1.5$ are chosen. The filter used in the sponge zone is of second order with d_0=1/2 and d_1=−1/4. In the last grid line (i=N), this filter is applied laterally to the boundary, but a one order filter is used perpendicularly.

The vorticity fields $|\omega_3|$ obtained in the (Ox_1x_2) plane with and without sponge zone are presented in Figure 12 at $t = 50$ and $t = 100$. As expected, the vortex is convected by the mean flow and reaches the outflow boundary at $t = 100$. At $t = 50$, the vortex has just come into the damping region, and no significant differences are detected because of the exponential progression of the magnitude of the filtering. However, when the vortex reaches the outflow boundary at $t = 100$, the vorticity is about two times smaller with the sponge zone than without. This can be evaluated more precisely with the vorticity profiles of Figure 13.

The pressure fields $|p'|$ obtained in the (Ox_1x_2) plane are presented in Figure 14 at $t = 100$ and $t = 200$. In Figures 14(a), without artificial damping, a single acoustic wave is generated by the exit of the vortex, and propagates upstream with an amplitude at $t = 200$ around

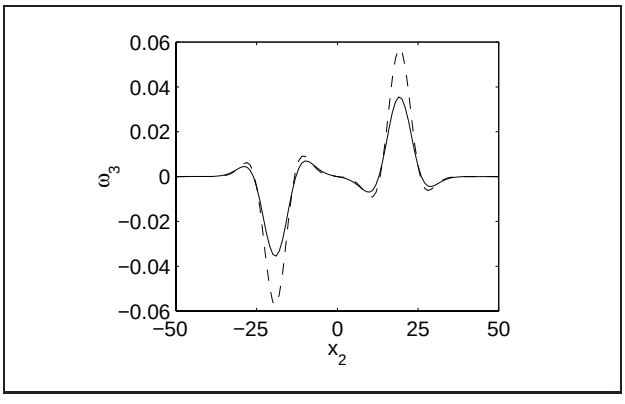

Figure 13. Application of a damping zone. Vorticity profiles for $x_1 = 50$ and $x_3 = 0$, obtained from LEE at $t = 100$: ——— with damping zone and − − − without damping zone.

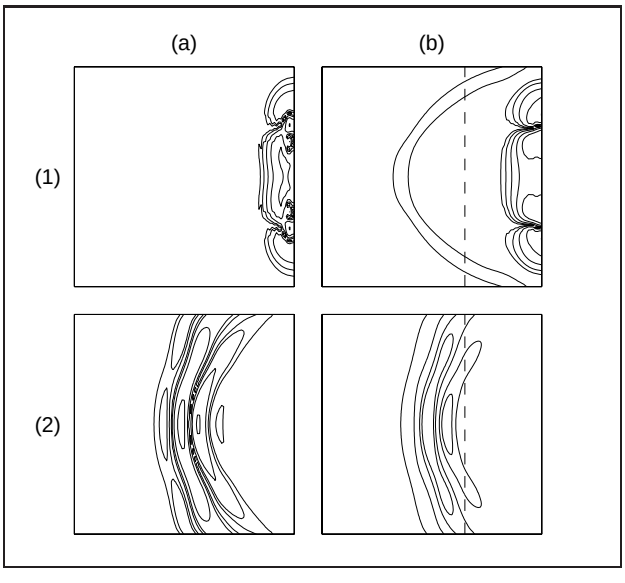

Figure 14. Application of a damping zone. Pressure fields $|p'|$ obtained in the (Ox_1x_2) plane from LEE: (a) without damping zone and (b) with damping zone at: (1) $t = 100$ and (2) $t = 200$. Representation of the 5 pressure iso-contours defined in Figure 10. − − − boundary of the damping zone.

$|p'| \simeq 4 \times 10^{-5}$. In Figures 14(b), using the artificial damping, two spurious acoustic waves are observed respectively at $t = 100$ and $t = 200$. The first one is produced when the vortex comes into the damping zone. The second one is generated by the vortex exit, and it is partially dissipated in the damping region during its upstream propagation. The amplitudes of the two waves in the physical domain, for $x_1 < 15$, are around $|p'| \simeq 1.5 \times 10^{-5}$. They are smaller than the amplitude of the reflected wave obtained without damping zone.

To compare more quantitatively the reflected acoustic waves, the axial pressure profiles for $x_2 = x_3 = 0$ are shown in Figure 15(a) and 15(b), at $t = 100$ and $t = 200$. The spurious wave generated by the gradient of artificial damping can be seen in Figure 15(a) at about $x_1 = -20$, with an amplitude less than 10^{-5}. The wave issuing from the exit of the ring vortex appears clearly in

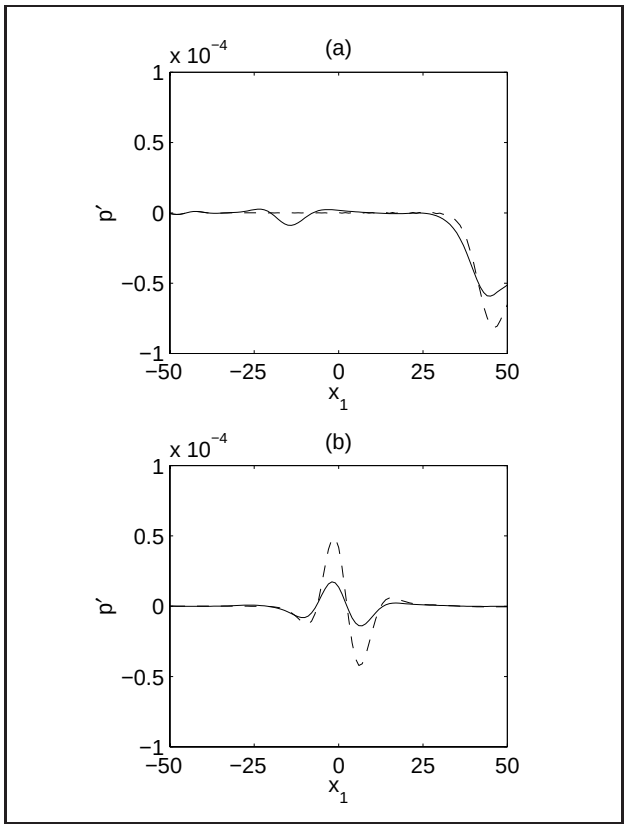

Figure 15. Application of a damping zone. Pressure profiles for $x_2 = x_3 = 0$, obtained from LEE at: (a) $t = 100$ and (b) $t = 200$. ——— with damping zone and – – – without damping zone.

Figure 15(b). The damping zone decreases its amplitude by a ratio around 3. This is very important with the aim of computing directly the physical acoustic field. In such computations [5, 6, 11], efficient damping zones must be built up by using a significant grid stretching in combination with an artificial damping similar the one experimented in this section.

5. Conclusion

Three-dimensional non-reflective boundary conditions are proposed in this paper following the work of Tam and his colleagues. Two test cases are also provided to evaluate and to optimize free field boundary conditions. They can be used for any simulation code to determine whether the boundary conditions are appropriate for aeroacoustic studies. With the far field boundary conditions, reflections generated by acoustic waves alone are negligible, whereas reflections generated by vortical structures are still to be treated using a damping zone because of the large amplitudes of flow disturbances compared to the amplitudes of sound waves. An example of damping zone is then shown to decrease the reflected waves in this case. More generally, the parameters of the damping zone, such as grid stretching and damping magnitude, should be adjusted to the characteristics of the simulated flow.

Appendix

A1. Analytical solution of the 3-D pressure pulse

To find the analytical solution of the sound field induced by an initial pressure pulse $g(r)$, the acoustical potential $\phi(r,t)$ is used. It is defined by $u = \nabla\phi$ and $p = -\partial\phi/\partial t$, and satisfies the wave equation, which writes, in spherical coordinates, as:

$$\frac{\partial^2\phi}{\partial t^2} - c_0^2 \frac{1}{r^2}\frac{\partial}{\partial r}\left(r^2\frac{\partial\phi}{\partial r}\right) = 0 \qquad \text{(A1)}$$

with initial conditions $\phi(r,0) = 0$ and $\partial\phi/\partial t\,(r,0) = -g(r)$.

In the same way as Morris in [25], the solution of this initial value problem can be determined by using the Hankel transform $\tilde{\phi}(\xi,t)$ defined by:

$$\begin{cases} \tilde{\phi}(\xi,t) = \dfrac{2}{\pi}\displaystyle\int_0^\infty r^2\phi(r,t)\,\mathrm{j}_0(\xi r)\;\mathrm{d}r \\ \\ \phi(r,t) = \displaystyle\int_0^\infty \xi^2\tilde{\phi}(\xi,t)\mathrm{j}_0(\xi r)\,\mathrm{d}\xi, \end{cases}$$

where $\mathrm{j}_0(z) = \sin(z)/z$ is the spherical Bessel function of the first kind and order 0, with properties given in [26]. This transform satisfies the following relation:

$$\frac{2}{\pi}\int_0^\infty r^2\frac{1}{r^2}\frac{\partial}{\partial r}\left(r^2\frac{\partial\phi}{\partial r}\right)\mathrm{j}_0(\xi r)\,dr = -\xi^2\tilde{\phi}(\xi).$$

Thus, by applying the Hankel transform to the wave equation (A1), we obtain:

$$\frac{\partial^2\tilde{\phi}}{\partial t^2} + c_0^2\xi^2\tilde{\phi} = 0$$

and $\tilde{\phi}(\xi,t)$ can be expressed as

$$\tilde{\phi}(\xi,t) = A(\xi)\cos(c_0t\xi) + B(\xi)\sin(c_0t\xi).$$

The initial conditions allows to find $A(\xi) = 0$ and $B(\xi) = -\tilde{g}(\xi)/\xi c_0$, that leads to:

$$\tilde{\phi}(\xi,t) = -\frac{\tilde{g}(\xi)}{\xi c_0}\sin(c_0t\xi)$$

and

$$\phi(r,t) = -\int_0^\infty \xi^2\frac{\tilde{g}(\xi)}{\xi c_0}\sin(c_0t\xi)\,\mathrm{j}_0(\xi r)\;\mathrm{d}\xi.$$

Pressure is then given by the following integral:

$$p(r,t) = \int_0^\infty \xi^2\tilde{g}(\xi)\cos(c_0t\xi)\,\mathrm{j}_0(\xi r)\;\mathrm{d}\xi.$$

In the first test case proposed in this paper, the pressure field is initialized by the Gaussian distribution $g(r) =$

$\exp\left(-\alpha r^2\right)$ whose corresponding Hankel transform is given in [27] by:

$$\tilde{g}(\xi) = \frac{1}{\beta} \exp\left(-\frac{\xi^2}{4\alpha}\right),$$

where $\beta = 2\alpha\sqrt{\pi\alpha}$. In a medium at rest, the pressure field produced by a Gaussian pulse takes the form:

$$p\,(r,t) = \frac{1}{\beta} \int_0^\infty \xi^2 \exp\left(-\frac{\xi^2}{4\alpha}\right) \cos\left(c_0 t\xi\right) \mathrm{j}_0\left(\xi r\right)\, \mathrm{d}\xi.$$

Acknowledgement

The authors wish to thank Ludovic Gréverie for the work during his master thesis. Computations have been performed on a Nec SX-5 of the Institut du Développement et des Ressources en Informatique Scientifique (IDRIS - CNRS).

References

[1] C. K. W. Tam: Computational aeroacoustics: issues and methods. AIAA Journal **33** (1995) 1788–1796.
[2] C. K. W. Tam: Advances in numerical boundary conditions for computational aeroacoustics. J. Comput. Acoust. **6** (1998) 377–402.
[3] S. K. Lele: Computational aeroacoustics: a review. Proc. 35th Aerospace Sciences Meeting & Exhibit, Reno, NV, 1997, AIAA Paper 97–0018.
[4] J. B. Freund: Acoustic sources in a turbulent jet: a direct numerical simulation study. Proc. 5th AIAA/CEAS Aeroacoustics Conference, Seattle, WA, 1999, AIAA Paper 99–1858.
[5] C. Bogey, C. Bailly, D. Juvé: Numerical simulation of the sound generated by vortex pairing in a mixing layer. AIAA Journal **38** (2000) 2210–2218.
[6] C. Bogey, C. Bailly, D. Juvé: Computation of the sound radiated by a 3-D jet using Large Eddy Simulation. Proc. 6th AIAA/CEAS Aeroacoustics Conference, Lahaina, HA, 2000, AIAA Paper 2000–2009.
[7] K. W. Thompson: Time dependent boundary conditions for hyperbolic systems, I. J. Comput. Phys. **68** (1987) 1–24.
[8] K. W. Thompson: Time dependent boundary conditions for hyperbolic systems, II. J. Comput. Phys. **89** (1990) 439–461.
[9] T. J. Poinsot, S. K. Lele: Boundary conditions for direct simulations of compressible viscous flows. J. Comput. Phys. **101** (1992) 104–129.
[10] M. B. Giles: Non-reflecting boundary conditions for Euler equations calculations. AIAA Journal **28** (1990) 2050–2058.
[11] T. Colonius, S. K. Lele, P. Moin: Boundary conditions for direct computation of aerodynamic sound generation. AIAA Journal **31** (1993) 1574–1582.
[12] A. Bayliss, E. Turkel: Far-field boundary conditions for compressible flows. J. Comput. Physics **48** (1982) 182–199.
[13] C. K. W. Tam, J. C. Webb: Dispersion-Relation-Preserving finite difference schemes for computational acoustics. J. Comput. Phys. **107** (1993) 262–281.
[14] C. K. W. Tam, Z. Dong: Radiation and outflow boundary conditions for direct computation of acoustic and flow disturbances in a nonuniform mean flow. J. Comput. Acoust. **4** (1996) 175–201.
[15] R. Hixon, S. H. Shih, R. R. Mankbadi: Evaluation of boundary conditions for computational aeroacoustics. AIAA Journal **33** (1995) 2006–2012.
[16] J. C. Hardin, J. R. Ristorcelli, C. K. W. Tam: Workshop on benchmark problems in computational aeroacoustics. NASA Conference Publication 3300, Icase / NASA, 1995.
[17] C. K. W. Tam, J. C. Hardin: Second workshop on benchmark problems in computational aeroacoustics. NASA Conference Publication 3352, Icase / NASA, 1997.
[18] NASA: Third computational aeroacoustics workshop on benchmark problems. NASA Conference Publication 209790, NASA, 1999.
[19] C. Bogey: Calcul direct du bruit aérodynamique et validation de modèles acoustiques hybrides. PhD Dissertation, Ecole Centrale de Lyon, n$^{\mathrm{o}}$ 2000-11, 2000.
[20] C. Bailly, D. Juvé: Numerical solution of acoustic propagation problems using linearized euler's equations. AIAA Journal **38** (2000) 22–29.
[21] C. K. W. Tam, Z. Dong: Wall boundary conditions for high-order finite-difference schemes in computational aeroacoustics. Theoret. Comput. Fluid Dynamics **6** (1994) 303–322.
[22] J.-P. Berenger: A perfectly matched layer for the absorption of electromagnetic waves. J. Comput. Phys. **114** (1994) 185–200.
[23] F. H. Hu: On absorbing boundary conditions for linerized Euler equations by a perfectly matched layer. J. Comput. Phys. **129** (1996) 201–219.
[24] C. K. W. Tam, L. Auriault, F. Cambuli: Perfectly matched layer as an absorbing boundary condition for the Linearized Euler Equations in open and ducted domains. J. Comput. Phys. **144** (1998) 213–234.
[25] P. J. Morris: Scaterring of sound from a spatially distributed, spherically symmetric source by a sphere. J. Acoust. Soc. Am. **98** (1995) 3536–3539.
[26] M. Abramowitz, I. A. Stegun: Handbook of mathematical functions. Dover, New York, 1965.
[27] I. S. Gradshteyn, I. M. Ryzhik: Table of integrals, series and products. Academic Press, 1980.